D68

9.1A FURTHER DEVELOPMENTS OF EISCAT AS AN MST RADAR

J. Rottger*

EISCAT Scientific Association
S-981 27 Kiruna, Sweden

INTRODUCTION

The principal capabilities of EISCAT as an MST radar were described in an earlier report by ROTTGER et al. (1983). Since the VHF transmitter of the EISCAT system is not yet delivered, only the UHF system could be used for radar experiments. Considerable developments in the year 1983 have now strongly improved the reliability of the operations. Most of the experiments were and will be done to investigate the high latitude ionosphere and thermosphere, but some time was also devoted to observations of the lower and middle atmosphere, particularly during the MAP/WINE campaign.

Modifications and a general refurbushing of the UHF transmitter now allows its reliable and continuous operation at maximum power levels of 1.5 MW. The transmit-receive response of the system was speeded up, shifting the shortest ranges to be sampled to less than 100 μs. Essential work was also done to reduce 50 Hz-hum insertions, and oscillator sidebands are acceptably suppressed now. Fairly unique pulse modulation patterns were implemented which apply multipulse schemes. By using the multifrequency/multichannel capabilities of the EISCAT system, highest efficiency at best spatial and temporal resolution can be achieved for D- and E-region work (TURUNEN and SILEN, 1984). Although the full spectrum information of D-region incoherent scatter signals can be achieved only by pulse-to-pulse sampling, the multipulse schemes can also be used to obtain adequate velocity estimates down to 75-80 km. For troposphere and stratosphere work only the pulse-to-pulse technique is applicable. However, restrictions exist for sounding the lower atmosphere because of exceptional ground clutter and the very limited size of the result memory of the correlator (2 k). In the following part we will present some typical examples of tropospheric and mesospheric data records to elucidate capabilities and limitations of the monostatic system. Bi- or tristatic operations are not feasible for troposphere investigations (because of mountain shielding in Tromso), they were, however, done to complement velocity measurements in the mesosphere and lower thermosphere. They also can be done to probe the lower (and middle) stratosphere.

TROPOSPHERE-STRATOSPHERE OBSERVATIONS

In Figure 1 examples of real-time displays (RTGRAPH) of the complex autocorrelation functions (ACF) and the corresponding spectra are shown. The first gate is at a range r = 15 km (corresponding to 100 μs), and the separation of the gates is 1.5 km (matched to the transmitted pulse length). At the chosen elevation angle 20° the corresponding lowest altitude is z = 5.1 km and the altitude steps (altitude resolution) are 0.5 km. During these experiments 64-point ACFs were computed on-line, using a pulse-to-pulse correlator program. The size of the result memory of 2 k words (a 64 bits) limited the number of range gates to 30 (including one background noise gate) and one gate for noise calibration. The transmitter was run at about 1 MW and 1 ms (2 ms) repetition rates, corresponding to a duty cycle of 1 (0.5) % when using a 10 μs pulse on a single frequency. In order to sample the troposphere and lower stratosphere the elevation angle was set to 20°. Higher elevation angles would be more suitable; this, however, can only be done after further work to improve the transmit-receive transition has been finished.

*presently at Arecibo Observatory, Arecibo, Puerto Rico, on leave from Max-Planck-Institut fur Aeronomie, Lindau, W. Germany.

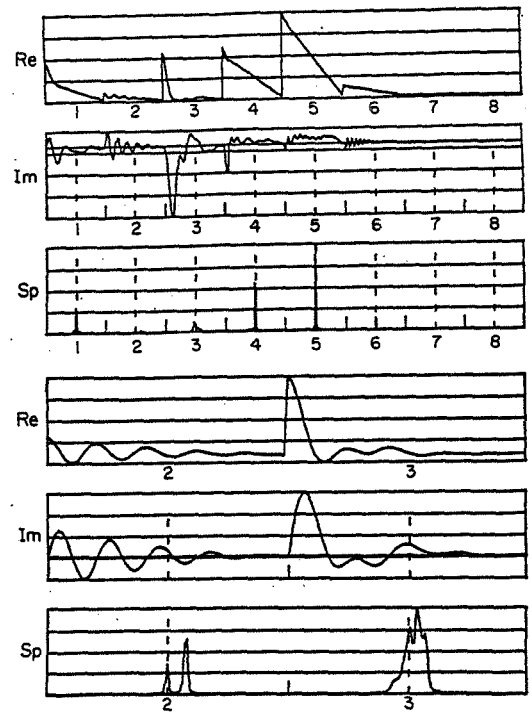

Figure 1. RTGRAPH displays of the real (Re) and imaginary (Im) part of the autocorrelation functions for different range gates (numbers) and the corresponding spectra (Sp) of echoes from short ranges (15-25 km).

The triangle shape of the real part of the ACF (e.g., gates 1, 4, 5, and 6) indicates a strong dc signal due to ground clutter, which appears as a spike at zero Doppler frequency in the spectra. The oscillating imaginary part indicates that besides the ground clutter also a signal with a Doppler shift was detected which is due to scatter from atmospheric turbulence. For elucidation of this fact two range gates with low ground clutter strength are displayed in the lower portion of Figure 1.

The ground clutter represents a very troublesome limitation to the investigations of the lower atmosphere with the monostatic UHF radar in Tromso. This clutter is obviously due to scatter/reflection from mountains. The Tromso system is in an area where high extending mountains are visible at distances from a kilometer out to several tens of kilometers. The antenna sidelobes, through which the clutter is received, cannot be suppressed. The only means would be to operate at higher elevation angles. Even then ground clutter is of considerable strength.

At 20° elevation angle the ground clutter is mostly stronger than the atmospheric signal which can be seen in Figure 2. The clutter also varies as a function of azimuth and range. The latter effect (seen also in Figure 1) is most cumbersome because the strongest clutter echo determines the attenuator setting of the receiver to avoid saturation effects. Because of the limited dynamic range of the receiver and the ADCs (8 bit), this could result in a

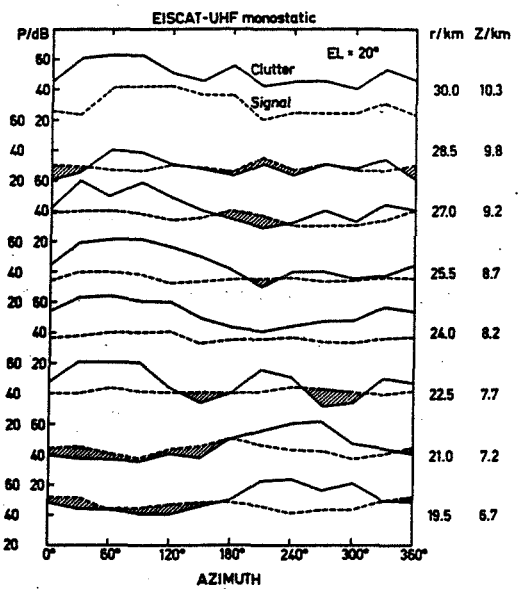

Figure 2. Ground clutter and signal power P as function of azimuth and range r. Shading indicates where the atmospheric signal was stronger than the ground clutter.

total attenuation of weak atmospheric signals, if the clutter-to-signal ratio is exceeding 48 dB.

At the relatively low average transmitter power of less than 8 kW and the 10 μs transmitter pulse, the signal-to-clutter ratio during the described operations at 20° elevation angle was not exceeding -20 dB at ranges larger than 30 km. This limited the observations to upper altitudes of about 10 km, which is the lower stratosphere in high latitudes. Using a long pulse/narrow bandwidth, lower elevation angle (i.e. longer ranges and thus less ground clutter) and almost maximum duty cycle, monostatic echoes up to heights above 20 km were recorded during EISCAT's first stratosphere experiments (ROTTGER, 1983).

The spectra shown in Figure 3 indicate another effect which complicates the analysis. This is the broadening or the modulation of the ground clutter signal. We assume that this may be either due to fading of the clutter signal or (digital) quantization noise. We do exclude a frequency or amplitude modulation of the transmitter or the receiver oscillators at these extended levels of -15 dB below the carrier signal.

Although the signal-to-clutter ratio is mostly less than one, some valuable results can be obtained which are briefly summarized in Figures 4-7. Using the VAD technique height profiles of wind velocity can be obtained and the fast real-time data acquisition allows to study high time resolution developments of clear-air turbulence. Similar measurements with the Millstone Hill Radar proved to be very useful (WATKINS and WAND, 1981; WAND et al., 1983).

OBSERVATIONS OF THE MESOSPHERE AND LOWER THERMOSPHERE

First incoherent-scatter observations of the D region were done in summer

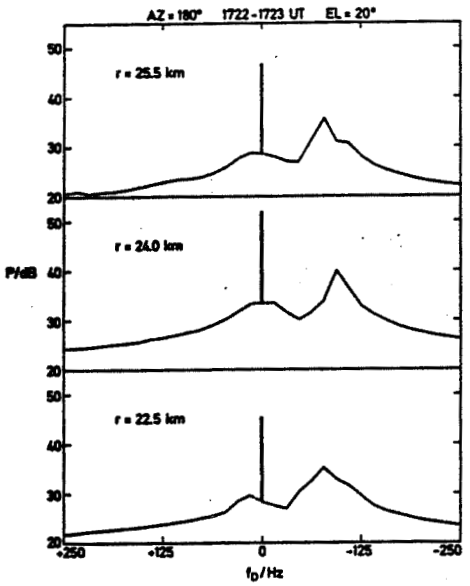

Figure 3. Doppler spectra showing ground clutter line at f_D = 0 Hz, a broadening of this line at levels of about -15 dB and the signal, shifted by about 100 Hz.

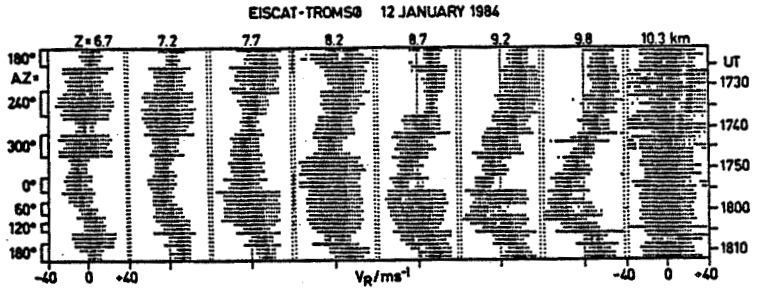

Figure 4. Velocity-azimuth-display (VAD) for altitudes z = 6.7 - 10.3 km. Note the variation of azimuth is not constant with time.

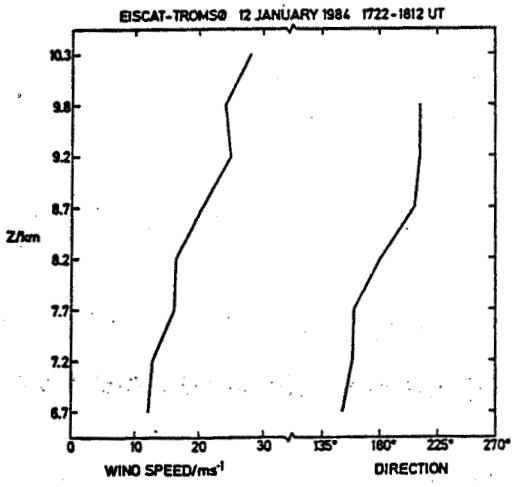

Figure 5. Wind speed and direction deduced from the VAD measurement shown in Figure 4.

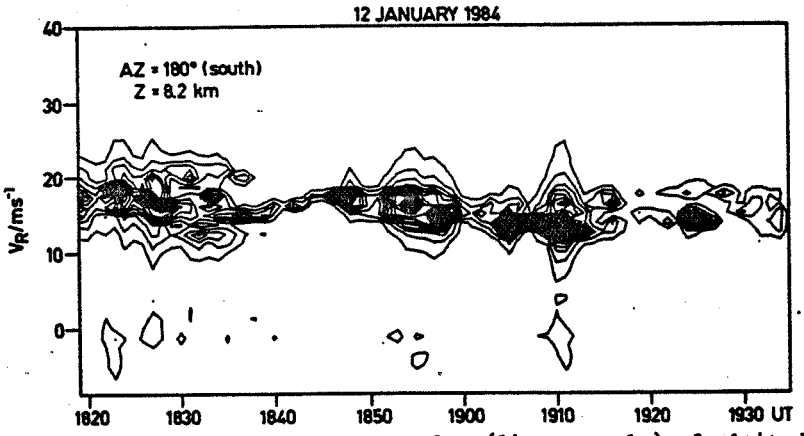

Figure 6. Spectrum contour plot (linear scale) of altitude gate z = 8.2 km, showing variability of the echo in power, Doppler shift and Doppler spread, due to intermittent clear-air turbulence carried through the radar volume.

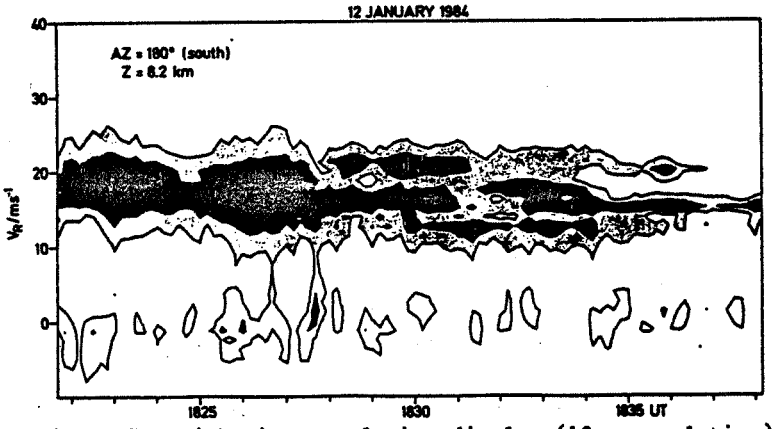

Figure 7. High time resolution display (10 s resolution) of clear air turbulence structure. Display is in logarithmic scale, where differences between contour lines are 3 dB. Note the splitting into patches with different velocities after 1830 UT.

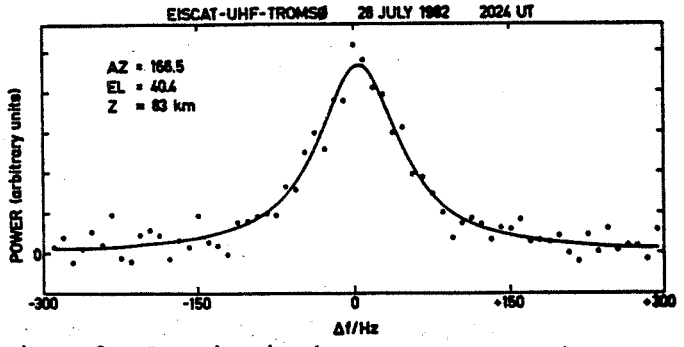

Figure 8. D-region incoherent scatter spectrum averaged over 2 min (from KOFFMAN et al., 1984).

1982 and a longer series of data were recorded during the MAP/CAMP campaign in July/August 1982. The relevant results of these campaign operations, namely electron density and wind profiles as well as mesopause temperature and negative-ion-to-electron ratios, were summarized by KOFMAN et al. (1984). In Figure 8 we show an example of an incoherent-scatter spectrum which could be obtained if high energy particle precipitation generates sufficient D-region ionization ($\gtrsim 10^{10}$ electrons per m^3), whereas the normal daylight D-region ionizations is not sufficient to yield evaluable signals. Because of the dominating collisions, the incoherent spectrum information of the D region and the lower E region up to about 110 km can be used to deduce neutral wind profiles and, under some assumptions, of the ion-neutral collision frequency, and also the neutral temperature.

The spectral width increases with height because of the decreasing collision frequency as shown in Figure 9. Above 92 km it is broader than 300 Hz. To resolve this spectrum the signal must be sampled at least at a rate of 667 μs. Applying the pulse-to-pulse sampling scheme, this rate is equal to the transmitter interpulse period (IPP). The EISCAT UHF transmitter does not allow a higher IPP than 1000 μs which places a limit to the maximum height where the pulse-to-pulse scheme can be applied. More restrictive, however, is the fact that the interpulse period must be longer than the range of the sampled gate. Since 667 μs corresponds to a range (= altitude at vertical incidence) of 100 km, the pulse-to-pulse scheme can no more be applied above about 92 km.

The altitude resolution in the region of the mesosphere and the lower thermosphere up to 130-150 km has to be of the order of some kilometer. Spectrum information above 92 km, thus, cannot be obtained with a long pulse (as possible in the F region) but only by applying multipulse schemes. It is evident that two explicitly different modulation schemes have to be used below 92 km and above 92 km. The pulse-to-pulse (< 92 km) and the multipulse (> 92 km) schemes, cannot be operated simultaneously or alternately with the present EISCAT radar controller/correlator system. However, as will be pointed out, the multipulse scheme can also be used to deduce the first spectral moment (Doppler shift to determine wind velocities) of mesospheric signals. Since the

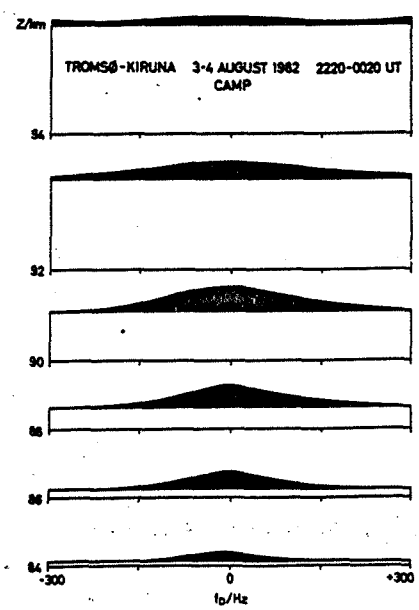

Figure 9. Average spectra (2220-0020 UT) of signals received in the bistatic mode at Kiruna during the CAMP rocket launches. The darkened area of the spectra is assumed to be due to the signal from the indicated heights, whereas the rectangular pedestal is due to signals picked up through antenna sidelobes from strong E-region ionization.

power profile (electron density) can be obtained directly from single pulse measurements, the additional application of the multipulse scheme allows to cover both the mesosphere and the lower themosphere.

Very powerful multipulse modulation schemes were recently developed by TURUNEN and SILEN (1984) and successfully applied in operations. These schemes make use of the unique multifrequency/multichannel capabilities of the EISCAT system; they allow to utilize the full applicable duty cycle at optimum range resolution and improve the significance of spectral estimates because of multichannel operation.

One of these schemes, shown in Figure 10, was used for mesosphere and lower thermosphere investigations during the MAP/WINE operations of EISCAT. This 4-pulse multipulse pattern yields the lags 1-6 of the ACF at lag increments of 40 μs. Four multipulse series are transmitted at frequencies F1, F2, F3 and F4. The EISCAT system allows to transmit on 16 frequencies at spacings of n 500 kHz around the center frequency 933.5 MHz and the reception on 8 channels, corresponding to the transmitted frequencies. The zero lag (power estimate) is obtained by using single pulses at frequencies F5 and F6.

The maximum lag of the multipulse ACF of 240 μs is obviously not sufficient to yield the full spectrum information at altitudes below about 100 km because the signal correlation time (inverse of spectral width) is longer than 240 μs. This is indicated in Figure 11 where the normalized real part ρ' of the ACFs at lags $\tau_1 = 40$ μs to $\tau_6 = 240$ μs is shown for different heights. For convenience of the display, the real part ρ' is normalized by $\rho(\tau_1)$, which is shown in relative units on the right-hand-side diagram of Figure 11. (For full ACF analysis the zero lag estimate, deduced by parabolic extrapolation, full ACF fitting or from the power profile has to be used.) In the center diagram the phase ϕ of the ACF (ϕ = arctan (Im(ACF)/Re(ACF))) is displayed. The phase derivative near zero lag is directly proportional to the Doppler shift $f_D = \phi(\tau)/2\pi\tau$. The linear phase variation at heights below 100 km indicates that we can use the phase information to deduce the Doppler shift. To improve the significance we have used all lags and calculated a weighted average

$$\bar{\phi} = \frac{\sum_{n=1}^{6} \phi(\tau_n) \cdot \rho(\tau_n)/n}{\sum_{n=1}^{6} \rho(\tau_n)}$$

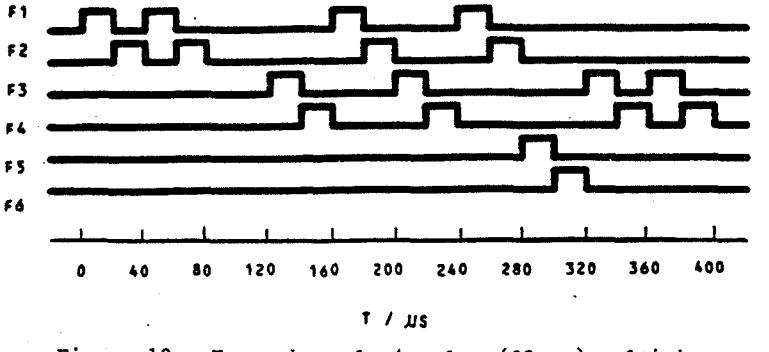

Figure 10. Four channels-4 pulse (20 μs) multiphase (F1, F2, F3, F4) and 2 channels single pulse (20 μs) at F5 and F6. Due to instrumental setting the frequencies F can be different to those noted.

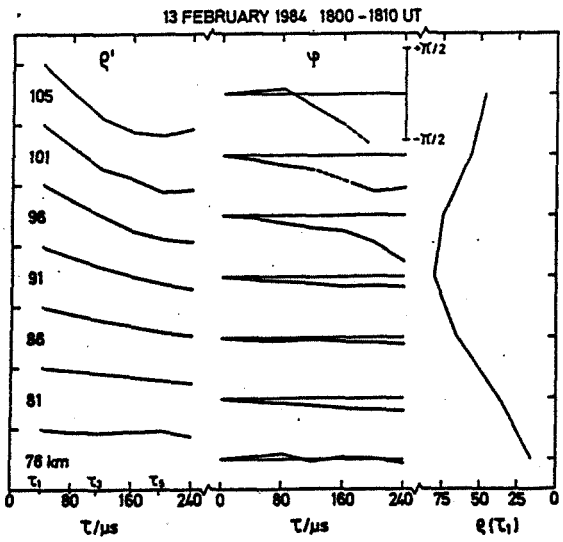

Figure 11. Normalized real part ρ' and phase ϕ of ACF, as well as the relative amplitude $\rho(\tau_1)$ of ACF at lag τ_1.

This yields a most reliable velocity estimate as long as the ACF does not cross zero.

We have used this approach to estimate preliminary velocity profiles which are shown in the Figures 12 and 13. During these operations the transmitter peak power was about 1.2 MW and the range resolution 3 km. The antenna was pointed at 33° elevation angle (corresponding altitude resolution 1.6 km) towards west (mesosphere gates north of Andenes Rocket Range) to measure the zonal wind component U and towards south to measure the meridional wind component V. Additionally the relative electron density profiles N_e' (uncalibrated) and the weighting function $\gamma = \Sigma\rho(\tau_n)$ are displayed. The relative amplitude of the weighting function is a measure for the significance of the velocity estimate. Because of the zero crossing of the ACFs, the velocity values above 100 km can be underestimated (this has to be corrected in the full spectral analysis to be applied later). The velocity profiles are additionally smoothly filtered by a five-point Hamming window. The open circles (e.g. in the V-profile measured from 1921-1930 UT on 31 Jan. 84) indicate preliminary velocity data obtained with chaff measurements (by courtesy of H. U. Widdel and U. von Zahn). The similarity of chaff and radar data, as well as the consistency of consecutive radar wind profiles, gain confidence in our method to determine mesosphere/lower thermosphere winds with the EISCAT UHF radar. In Figure 13 a time series of the zonal wind component is shown and also compared with quasi-simultaneous chaff measurements (MC8, 9, 10). The radar profiles clearly show a downward progressing wave structure with period of about 2-4 hours and vertical wavelength of 10-20 km. The wave amplitude evidently increases with altitude. However, one has to take into account that electrodynamical effects influence the structure of the measured ion drift velocity above about 110 km. A similar wave event was earlier observed with the Pokerflat MST radar in the altitude region 60-80 km (BALSLEY et al., 1983).

Finally, in Figure 14 a plot of electron density measured during a high energy particle precipitation event is shown. It proves that the sensitivity of the EISCAT UHF radar is sufficient to measure D-region (mesosphere) signals

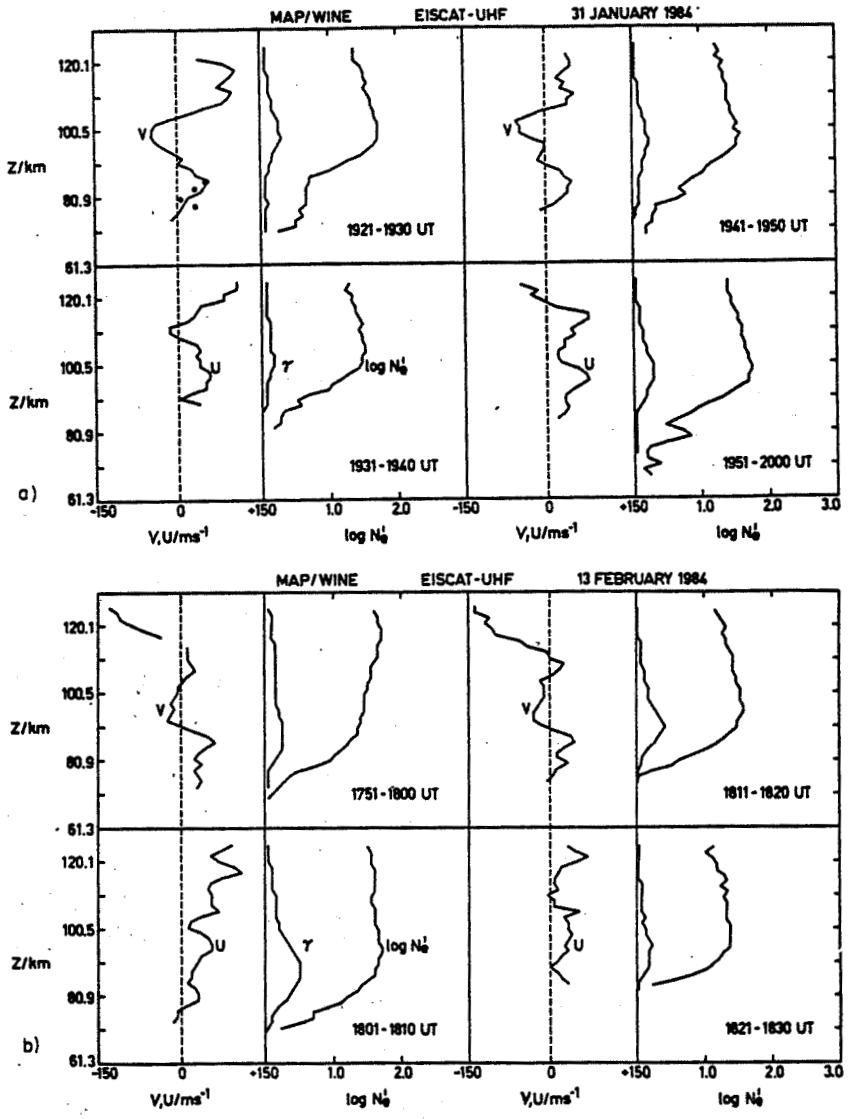

Figure 12. Profiles of zonal (U) and meridional (V) wind velocities, and relative electron density N_e' as well as the weighting function γ.

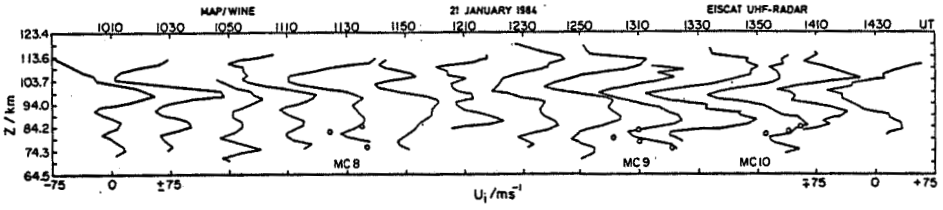

Figure 13. Time series of zonal winds. The open circles denote chaff wind data (courtesy of H. U. Widdel and U. von Zahn).

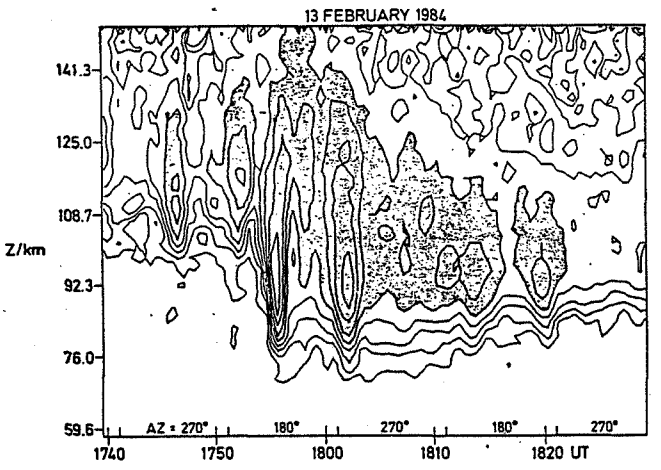

Figure 14. Electron density contour plot; the contour steps are 1.5 dB. Note the high time resolution of 30 s, which allows detection of highly variable electron density structures.

during appropriate geophysical conditions. Similar measurements at other incoherent-scatter radar facilities applying multipulse/multichannel operations for mesosphere/lower thermosphere investigations are not known yet.

I acknowledge the pleasing and very efficient cooperation with all EISCAT staff members.

The EISCAT Scientific Association is funded and operated by Centre National de la Recherche Scientifique, France, (CNRS)
Suomen Akatemia, Finland, (SA)
Max-Planck Gesellschaft, West Germany, (MPG)
Norges Almenvitenskapelige Forskningsrad, Norway, (NAVF)
Naturvetenskapliga Forskningsradet, Sweden, (NFR)
Science and Engineering Research Council, UK, (SERC).

REFERENCES

Balsley, B. B., W. L. Ecklund and D. C. Fritts (1983), Mesospheric radar echoes at Poker Flat, Alaska: Evidence for seasonally dependent generation mechanism, Radio Sci., 18, 1053-1058.

Kofman, W., F. Bertin, J. Rottger, A. Cremieu, P. J. S. Williams (1984), The EISCAT mesospheric measurements during the CAMP campaign, J. Atmos. Terr. Phys., 46, in press.

Rottger, J. (1983), Some capabilities of the EISCAT UHF radar for investigations of the stratosphere, Preprint Vol. 21st Conf. on Radar Meteorology, American Meteorological Society, Boston/USA, 100-103.

Rottger, J., M. Baron and K. Folkestad (1983), Capabilities and limitations of EISCAT as an MST radar, Handbook for MAP, Vol. 9, SCOSTEP Secretariat, Dep. Elec. Eng., Univ. Il, Urbana.

Turunen, T. and J. Silen (1984), Modulation patterns for the EISCAT incoherent scatter radar, J. Atmos. Terr. Phys., 46, (in press).

Wand, R. H., P. K. Rastogi, B. J. Watkins and G. B. Loriot (1983), Fine doppler resolution observations of thin turbulence structures in the tropostratosphere at Millstone Hill, J. Geophys. Res., 88, 3851-3857.

Watkins, B. J. and R. H. Wand (1981), Observations of clear air turbulence and winds with the Millstone Hill radar, J. Geophys. Res., 86, 9605-9614.